Towards stiffness tunable programmable matter

Lupo Manes [a], Sebastiano Fichera [a], Paolo Paoletti [a,*]

[a]*School of Engineering, University of Liverpool, L69 3GH Liverpool, United Kingdom*

Abstract

The Datom is a novel design for a programmable matter robotic agent, proposed by Piranda and Bourgeois (2022), that can move and reconfigure by deforming its outer shell. This paper explores how the kinematic behaviour of the single Datom, paired with the stiffness of its actuators, can determine the stiffness of the structures the agents create. We propose a simplified mathematical model based on conservation of elastic energy that can characterise the stiffness of lattice structures created by Datoms. The model is validated experimentally to demonstrate that it provides good predictions, especially as the size of the lattice increases. Furthermore, an implementation for a stiffness tunable reconfigurable lattice is proposed and a functioning proof-of-concept prototype is introduced in this paper.

Keywords: Cellular and Modular Robots, Compliant Joints and Mechanisms, Modeling, Control, and Learning for Soft Robots.

1. Introduction

The concept of modular robotics was first introduced in the late 1980s to describe a reconfigurable robotic system that can use a set of modules to achieve higher flexibility while compromising specificity

Lattice type modular robots still face many challenges because of the complexity they present, both at a physical and control level. The main challenge of the hardware is designing and manufacturing devices at cm and

---

*Corresponding author

Email addresses: L.Manes@liverpool.ac.uk (Lupo Manes),
S.Fichera@liverpool.ac.uk (Sebastiano Fichera), P.Paoletti@liverpool.ac.uk
(Paolo Paoletti)

mm scale capable of latching and actuating the movement relative to one another, while keeping it affordable

Almost all of the proposed architectures for programmable matter use fully rigid agents, which are easier to control during reconfiguration, but make it impossible to modify the stiffness of the final object without modifying its structure. However, the Datom architecture was recently proposed as a novel geometry for programmable matter agents

2. Datom design and manufacturing

This section briefly describes the main aspects of the Datom design firstly proposed in

It is also useful to think of the shell assembly as 3 rings made up of 4 A-faces and 4 C-faces, shown in Fig. 1b, with 1 ring for each Cartesian plane. The origin of the coordinate system is placed in the centre of the Datom and the axis pass through the centres of opposite A-faces. The core assembly contains the core and 6 actuators, coloured respectively yellow and silver. The original design proposes shape memory alloy springs to implement a bistable toggle linear actuator that can toggle between fully contracted and fully extended. Our implementation replaces the actuators with normal springs at first. This allows us to explore the passive behaviour of the agents and the lattices they can create. Successively springs are replaced with pneumatic actuator for the proof of concept device described in Section 5. All of the shell components have been 3D printed using PLA in a Ultimaker S5 FDM printer, except for the steel dowel pins that are used for the revolute joints

Datoms can pack in the three-dimensional space by connecting to other Datoms through the C-faces in all directions. This configuration forms a face-centred cubic lattice, as shown in Fig. 1c. When describing a lattice of Datoms, as shown in Fig. 1d, the size of the lattice in a given Cartesian direction is defined as the number of lattice units the lattice spans across that axis.

3. Datoms for stiffness tunable programmable matter

This section will cover how the Datoms mechanical structure can be harnessed to implement stiffness tunable programmable matter. Specifically, the kinematics of the Datom deformation will be characterised and will be used to express the relationship between the stiffness of individual Datoms and the stiffness of the structure they collectively form.
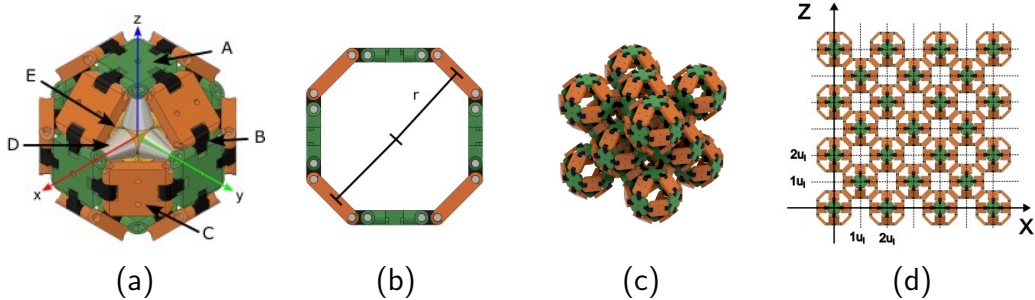
2

Figure 1: Details regarding the Datoms design and the structures the agents can create. (a) A single Datom with all it's components: A) A-face. B) Link. C) C-face. D) Actuator, E) Core. (b) Configuration of A-plates, C-plates and links making up a shell ring. The radius of the Datom is defined as half of the distance between opposing C-Faces. (c) Datoms connected together to form a a face centred cubic lattice. (d) Two-dimensional lattice lying on the XZ plane highlighting the spacing between Datoms.

3.1. Datom deformation modes

The Datom shell has two deformation modes, which can be identified based on the source of the force driving deformation: internal actuators or external agent/force.

We define Active Deformation, shown in Fig. 2a as the deformation caused from internal actuation, when an A-face is pulled towards the centre of the Datom by the connected actuator. This mode of deformation is the one that is used to move Datoms relative to one another and navigate around the structure.

We define Passive Deformation, shown in Fig. 2b as the deformation caused from an external force, which can be observed when the multiple Datoms connected together are subjected to an external force applied along one of the Cartesian axes. We are particularly interested in this mode, as it will allow us to develop a model for how the stiffness of the individual Datoms determines the stiffness of the lattice. For this mode, we have to further distinguish the behaviour of Datoms at the boundary of the structure and the ones that are fully surrounded by other Datoms. The latter behaviour is characterised in section 3.3.

3.2. Lattice boundary stiffness

The Datoms at the boundaries of the lattice behave differently than the ones on the inside. The springs connected to the A-faces facing out of the

3

(a)

(b)

Figure 2: Representation of the two possible modes in which datoms can deform. A) Active deformation where the actuator is fully retracted and pull the A-face into the core causing the surrounding C-faces to lie on the same plane. B) Passive deformation caused by an external force which will cause a movement of the dome until the limits of the joints are reached.

lattice all react independently to an external force, as they are not mechanically coupled to any other spring in the lattice. Also, the force transfers to the spring through the A-face linearly, meaning the stiffness of the half dome exposed at the boundary of the lattice is simply the stiffness of the internal spring.

3.3. Lattice bulk stiffness

This section will discuss the relation between the stiffness and deformation of the Datom and the stiffness of the lattice. For the purpose of this initial study, we consider the Datoms and the lattice to be ideal, using the following sets of assumptions: i) all the bodies are perfectly rigid, ii) all the joints have no mechanical play or backlash, iii) all connections between adjacent C-faces are perfectly rigid, and iv) the system is frictionless.

3.3.1. Deformation Kinematics

When an external force is applied to the lattice, it is transferred from Datom to Datom through the C-plates. The applied force will then cause the internal springs to deform. If a force is applied along one of the Cartesian axes, all the Datoms in the lattice will deform uniformly. We can therefore perform our analysis on an individual Datom at first. The first thing to note is that the shell-ring normal to the force is minimally affected; This is because all of the A-faces of the shell ring are being pushed outwards radially from the

centre of the Datom by the moving linkages but cannot move because of the kinematic constraints designed into the joints discussed in Sec. 2. Therefore the shell ring normal to the force is considered rigid for the purpose of our analysis. Moreover, the remaining 2 shell-rings deform uniformly due to the radial symmetry of the Datom and of the loading conditions. We can therefore analyse the deformation on one quarter of one of the shell-ring, as shown in Fig. 3. In this scenario, forces are transmitted through the lattice via the C-faces.
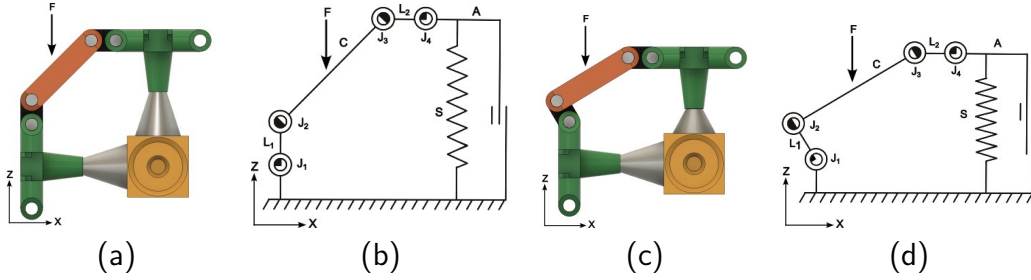

Figure 3: Section of the Datom taken into account for the kinematic study. In the free body diagrams the revolution limits for the revolution joints are represented by the angle of the white sector of the circle placed on the joint. (a) Component view at rest. (b) FBD at rest. (c) Component view compressed. (d) FBD compressed.

For the purpose of our analysis, the origin of the coordinate system is placed at the centre of revolution of joint J_1. The dimension of all the Datom's components, the faces and the links whose length is defined in Eqs (1) and (2) respectively, are related to its radius (r), which is defined as the half distance between two opposite C-faces. All thes parameters are given in

$$\overline{L_1} = \overline{L_2} = r\frac{2 - \sqrt{2}}{3\sqrt{2} - 1} = l \tag{1}$$

$$\overline{C} = r\frac{2}{3\sqrt{2} - 1} = f \tag{2}$$

A force F applied to the C-face, as shown in Fig. 3d and 3c, causes J_3 to move in the negative z direction, and due to the rotation limits in place in J_4, the joint J_4 does not rotate. Therefore, L_2 and A act as a single body constrained prismatically along the z direction. We can then characterise

5

the system based on the angles of J_1 and J_2, while knowing that the end of C, which is coincident with J_3, is constrained to only move along the z with the ordinate value constrained between 0 and f. The angles for $J_{1\Theta}$ and $J_{2\Theta}$ can be derived by using the geometric solution for the inverse kinematics of a link serial robot

$$J_3 = (f * \cos \frac{\pi}{4}, 0 \le z \le f) \tag{3}$$

$$J_{2\Theta} = \cos^{-1} \frac{x^2 + z^2 - l^2 - c^2}{2lc} \tag{4}$$

$$J_{1\Theta} = \tan^{-1} \frac{x}{z} + \tan^{-1} \frac{c \sin J_{2\Theta}}{l + c \cos J_{2\Theta}} \tag{5}$$

These equations can be solved for a fixed $x = f * \cos \frac{\pi}{4}$ and the resulting z represents the length of the spring.

The last factor to consider is the revolution constraints of the joint J_2. Specifically, $J_{2\Theta}$ is constrained between $\pi/2$ and $3\pi/2$. Solving Eq: (4) for $J_{2\Theta} = \frac{\pi}{2}$ gives us a spring extension of $\approx 0.449r$. This means that when a force is applied to the C-face the spring can compress to a maximum of 23% compared to when the mechanism is at rest and spring length is $\approx 0.616r$.

3.3.2. Datom stiffness from kinematics

The kinematics of the individual Datom can be applied to all of the other Datoms in the lattice if the set of assumptions discussed in Section 3.3 is valid. From Fig. 4 we can observe that for each layer of Datoms, as the lattice is compressed, the distance between the rings normal to the stress changes. This value can be expressed as the normal component of the length of C plus 2 times the vertical component of L_1, i.e.

$$D = 2l \sin J_{1\Theta} + f \sin (J_{1\Theta} + J_{2\Theta}) \tag{6}$$

By utilising equations 4-5 we can characterise the deformation of a 2 level lattice against the spring resulting in the curve shown in Fig. 4c

This curve represents the relationship between the deformation of one tier of a Datom lattice and the deformation of the springs involved. We can see that the relationship can be represented linearly by a line with slope 0.898 and no intercept. The relationship between deformation of the lattice (Δ_l) and spring (Δ_s) can be used to calculate the stiffness of the lattice (K_l)
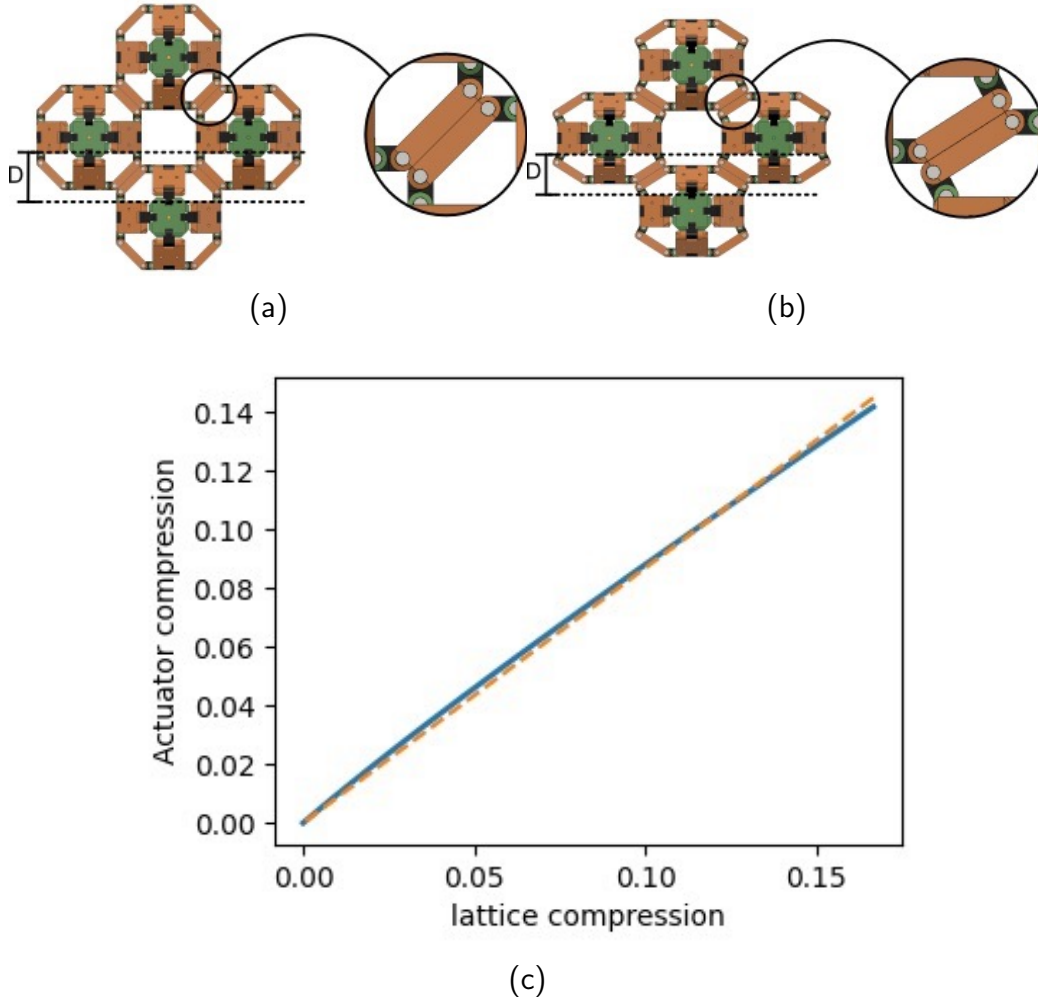
Figure 4: Relationship between lattice and actuator compression. Side by side view of the resting (a) and compressed (b) lattice. Magnification displays the change in distance between the shell ring normal to the compression. The graph (c) shows the Relationship between lattice compression $\left(\frac{\Delta_l}{r}\right)$ and Datom spring compression $\left(\frac{\Delta_s}{r}\right)$ and its linear approximation. Both axes have been divided by the radius of the Datom to make the graph dimensionless.

from the stiffness of the spring (K_s) through conservation of elastic energy. Indeed, under our assumptions, the energy stored in the lattice (U_l) must be equal to the energy stored in the spring (U_s), therefore

$$\begin{cases} U_l = U_s \\ U_l = \frac{1}{2}K_l\Delta_l^2 \\ U_s = \frac{1}{2}K_s\Delta_s^2 \\ \Delta_s = 0.898\Delta_l \end{cases} \tag{7}$$

.

$$\Rightarrow K_l = 0.898^2 K_s \tag{8}$$

3.3.3. Two-Dimensional lattice

Let us first consider a two-dimensional plane of ideal Datoms that follows the previous assumptions and is placed in the following scenario. The lattice lies on the XZ plane and spans D_x lattice units along the x axis and D_z along the z axis. A uniform force is applied in z direction. In this scenario, only the springs oriented along z are deformed. We can then calculate the stiffness of the lattice through conservation of energy. Indeed, that the elastic potential energy of the lattice (U_l) must be the sum of the elastic potential energy stored in the springs (U_s). The number of engaged springs (n_s) is given by

$$n_s = D_x \times (D_z - 1) \tag{9}$$

For a two-dimensional lattice, the relationship between Δ_l and Δ_s given in equation (7) needs to be expanded to account for the z dimension of the lattice, thus obtaining

$$\Delta_s = \frac{0.898}{D_z - 1}\Delta_l \tag{10}$$

which, in turns, implies that the stiffness of the two-dimensional lattice can be expressed as

$$K_l = K_s\frac{0.898^2 D_x}{D_z - 1} \tag{11}$$

3.3.4. Three-Dimensional lattice

The model discussed above can be expanded to three-dimensional lattices, by expanding the lattice in the remaining Cartesian direction and stacking more planes to form a face-centred cubic lattice. For the three-dimensional
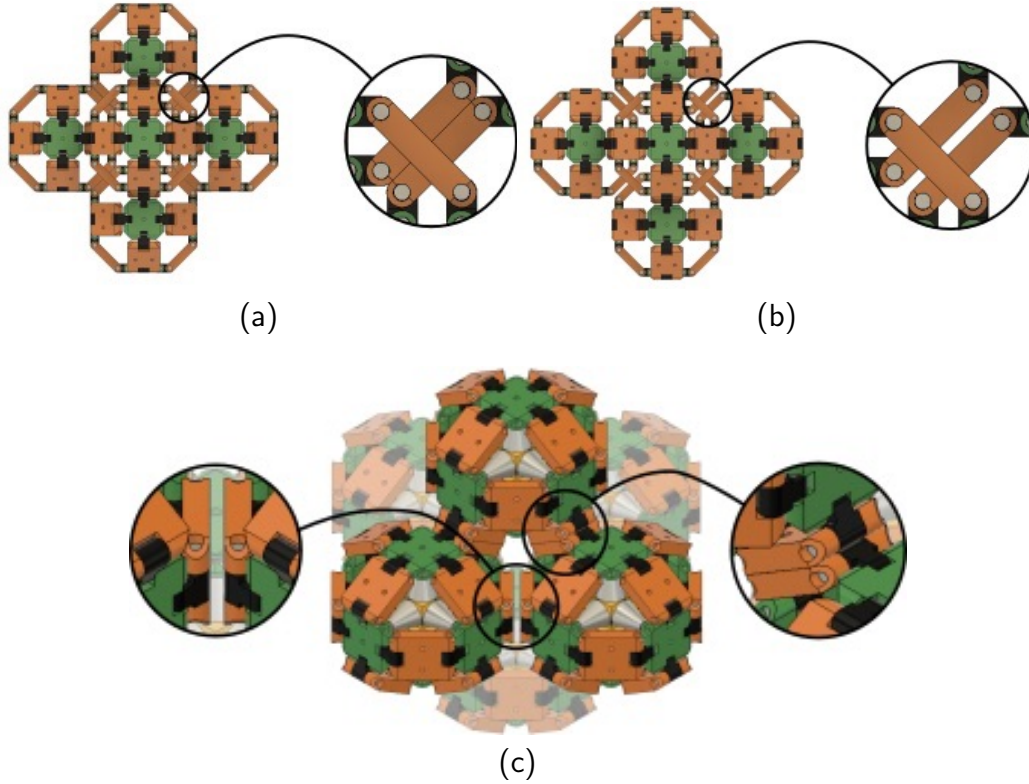
Figure 5: Side by side view of a section of 3D lattice compressed and at rest.(a) Render of a section of a three-dimensional lattice while at rest. All off the C-faces are in contact. (b) Render of a section of a three-dimensional lattice deformed by a force going into the page. The C-faces on the shell rings normal to the force have separated. (c) Perspective render of a deformed 3D lattice with zoomed details showing how the C-faces on the shell-ring normal the stress have disconnected to allow for the deformation and how the C-faces remain connected allowing for forces to transmit throught the lattice.

lattice to be able to deform, the Datoms in the lattice need to disconnect all C-faces belonging to the shell rings normal to the stress. This is necessary to allow the lattice to expand along the normal plane as it is compressed, as shown in Fig. 5. Forces can still be transferred from Datom to Datom through the remaining 8 C-faces maintaining connection to the Datom above and below in the lattice. We can adapt Eq. 11 to account for the dimension of the lattice in the y direction, represented by D_y, thus obtaining

$$K_l = K_s \frac{0.898^2 D_x D_y}{D_z - 1} \tag{12}$$

4. Experimental validation

The mathematical model introduced in Section 3 was experimentally validated by manufacturing lattices of Datoms' shells and performing uniaxial compression tests on them.

4.1. Specimen

The specimen was designed to simulate a Datom with a radius of 6 cm. To simplify manufacturing and reduce uncertainties due to spurious compression modes, the specimen was reduced to a two-dimensional representation, as shown in Fig. 6a. Such implementation also allowed it to fit it within the testing volume constraints of the Universal Testing Machine (UTM) used for the tests, and remove components potentially introducing unwanted friction. This representation uses vertical steel rods to retain the prismatic constraint of the A-faces and uses horizontal steel rods to maintain alignment for Datoms on the same horizontal plane. The addition of these guides will allow us to simulate the constraint of an infinite 2D lattice on a finite model. The model Datoms are connected to one another with screws for a rigid connection. The Datoms that are placed at the boundary of the lattice have a rigid half to remove the lattice boundary stiffness component from the experiment, as shown in Fig.6a. All components have been 3D printed to enable quick manufacturing, all revolute joint use steel dowel pins and lubrication to reduce friction and backlash in the assembly. The model removes 2 springs in each Datom, only keeping the vertical ones. The spring and faces that would have been part of the shell ring normal to the stress have been simplified to a rigid member as explained in Sec. 3.3.

4.2. Method

The experiments have been conducted using an Instron 3345 UTM equipped with a 5KN load cell. Tests have been conducted using three batches of springs (a, b, c) of different stiffness: $K_a = 0.37 N/m$, $K_b = 0.93 N/m$, $K_c = 2.48 N/m$. All springs in every batch have been tested and chosen so as to be within 5% of the nominal value. All experiments have been carried out with a loading speed of 1000 mm/min to reduce the influence of friction on

the system. Each spring has been tested with four different 2D lattice configurations: 3 by 2, 3 by 3, 3 by 4, and 3 by 5. Each specimen configuration has been tested ten times.
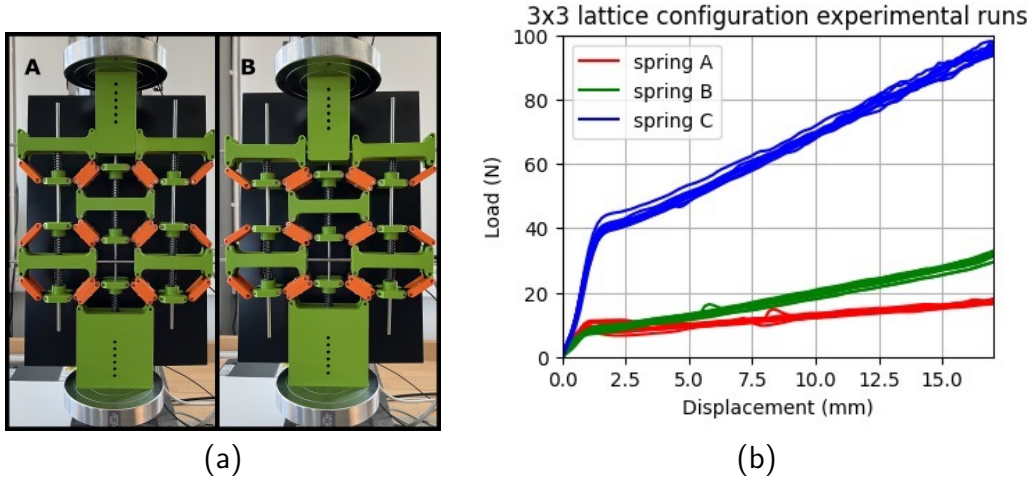

(a) (b)

Figure 6: Figures and graphs from the compression testing of the 2D lattice. (a) 3 by 4 lattice during testing with the Instron machine, at rest (A) and compressed (B). (b) Graph displaying the experimental results from the compression test for the 3 different spring in a 3 by 3 lattice. The lattice has clear linear stiffness.

4.3. Results

All specimens display linear behaviour within the movement limits dictated by the mechanism, see Fig. 6b. Furthermore, the data from the experiment has been post-processed to obtain stiffness values for all specimens. The post-processing consists of, firstly, removing data points at the beginning of the run where the specimen is settling, and secondly, fitting a line to the remaining points. The slope of that line is the stiffness of the specimen. The results for each specimen are averaged, and the mean is compared to the predicted specimen stiffness. All of the results are shown in Fig.7. We can observe that for smaller lattice configurations, the model under-predicts with a large error, but as the dimensions of the lattice increase the prediction approximates the characteristics of the lattice with progressively smaller error. The discrepancy between the prediction and the experimental results at smaller dimensions is due to the model not accounting for the behaviour of the agents at the boundary layer, which are less constrained and have some
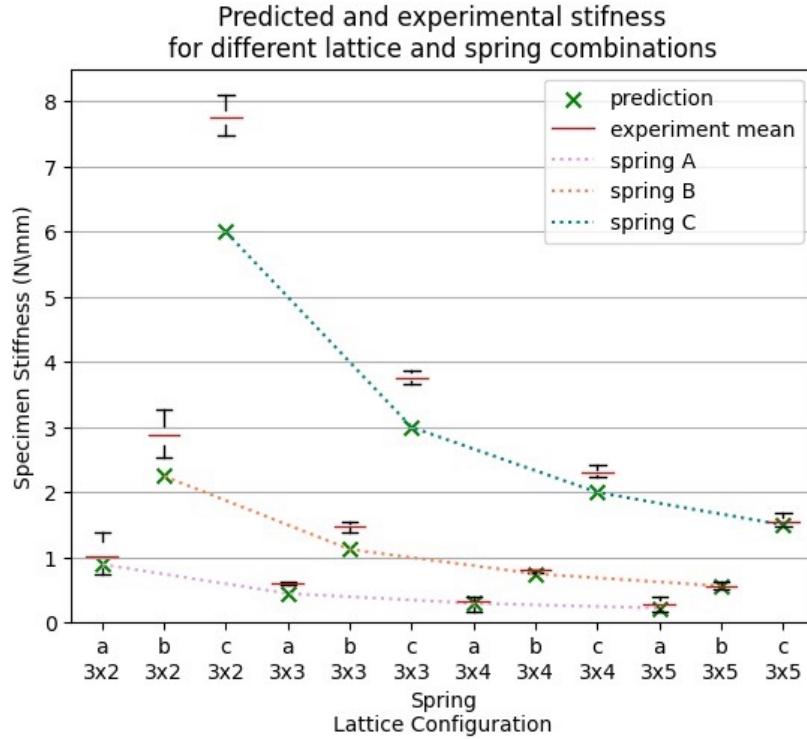
11

Figure 7: Results from 2D lattice test. The boxplot shows how the experimental values collected compare to the predicted stiffness values. As the dimension of the lattice increases, the prediction error decreases.

A-faces subject to twisting inducing the joints to seize. This behaviour becomes less prominent as the size of the lattice increases. As the final goal of programmable matter is to have an extremely dense arrangements of agents, the model provides a close approximation in those scenarios.

5. Proof of Concept for Stiffness Tunable Programmable Matter

This section proposes a potential design to demonstrate stiffness tunable programmable matter.

5.1. Specimen

Six Datom have been manufactured for the proof of concept. These Datoms have a radius of 6cm and have been connected to form a diamond
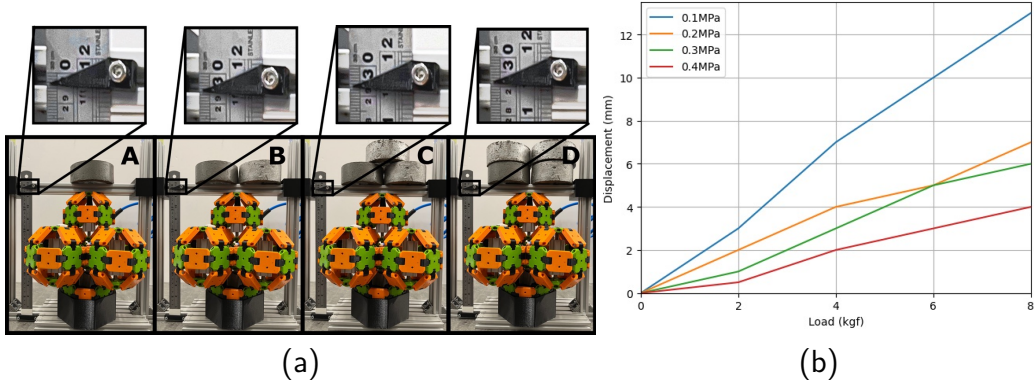
Figure 8: 3D lattice testing and results. (a) 3D lattice compression test. The figures show the proof of concept lattice at 0.3MPa actuator pressure and loaded with: A) 2kg B) 4kg C) 6kg D) 8kg. Those lead respectively to deflections of 1mm, 3mm, 5mm, and 6mm. (b) Force displacement curve of the lattice at different actuator pressures. The lattice behaves like a linear spring for the tested pressures.

configuration with one Datom at the bottom and one at the top of the lattice and 4 placed between them. 10 single action pneumatic cylinders, with a 16mm bore and 10mm travel (SMC CQ2B16-10S) in the normally retracted configuration, have been used to act as the variable stiffness actuators involved in the deformation caused from applied vertical stress. Therefore, the 4 Datoms in the middle layer have been fitted with 2 actuators each, while only one is used for the top and bottom Datoms. These allow the stiffness of the lattice to be modulated through the pressure in the chamber. The 10 actuators have been connected in parallel to a compressor so that all of the chamber are pressurised uniformly.

5.2. Method

The lattice has been placed in a fixture that allows for weights to be placed on top of the lattice, recording the deformation after reaching steady state. The actuators in the lattice have been pressurised to the following pressures of 0.1, 0.2, 0.3 and 0.4MPa, without any load placed on top. For each pressure value the resting lengths have been recorded and successively weights have been placed on top of the lattice, from 2kg to 8 kg in 2kg increments. The setup is displayed in Fig. 8a

5.3. Results

The experiment show that as the pressure in the actuator's chambers increases, so does the stiffness of the lattice. Indeed, the lattice stiffness at 0.1MPa is ~ 6.15N/mm and increases up to $\sim 20 N$/mm at 0.4MPa. The lattice also maintains a linear stiffness at the tested pressure values, as shown by Fig. 8b.

6. Conclusions

The mathematical model presented in this paper can be used to calculate the stiffness of a uniform Datom lattice with known dimensions under uniform loading conditions. This relationship is shown to be linear, which is highly advantageous for an implementation of the device for real world operations. The experimental results show that the model can be used to predict the stiffness of large lattices, massively simplifying the stiffness control of large lattice configurations. Following these findings, a proof of concept device consisting of 6 Datoms has been used to demonstrate that the stiffness of the lattice can be easily tuned using a pneumatic variable stiffness actuator. The device shows that the basic working principle is sound and confirms that the Datom architecture

References

[1] T. Fukuda and Y. Kawauchi, "Cellular robotic system (CEBOT) as one of the realization of self-organizing intelligent universal manipulator," in *Proceedings., IEEE International Conference on Robotics and Automation.* Cincinnati, OH, USA: IEEE Comput. Soc. Press, 1990, pp. 662–667.

[2] K. C. Wolfe, M. S. Moses, M. D. Kutzer, and G. S. Chirikjian, "M³Express: A low-cost independently-mobile reconfigurable modular robot," in *2012 IEEE International Conference on Robotics and Automation.* St Paul, MN, USA: IEEE, May 2012, pp. 2704–2710.

[3] M. Rubenstein, C. Ahler, and R. Nagpal, "Kilobot: A low cost scalable robot system for collective behaviors," in *2012 IEEE International Conference on Robotics and Automation.* St Paul, MN, USA: IEEE, May 2012, pp. 3293–3298.

[4] R. Fitch and Z. Butler, "Million Module March: Scalable Locomotion for Large Self-Reconfiguring Robots," *The International Journal of Robotics Research*, vol. 27, no. 3-4, pp. 331–343, Mar. 2008. [Online].

[5] J. Campbell and P. Pillai, "Collective Actuation," *The International Journal of Robotics Research*, vol. 27, no. 3-4, pp. 299–314, Mar. 2008.

[6] P. Holobut, M. Kursa, and J. Lengiewicz, "A class of microstructures for scalable collective actuation of Programmable Matter," in *2014 IEEE/RSJ International Conference on Intelligent Robots and Systems*. Chicago, IL, USA: IEEE, Sep. 2014, pp. 3919–3925.

[7] H. Bojinov, A. Casal, and T. Hogg, "Emergent structures in modular self-reconfigurable robots," in *Proceedings 2000 ICRA. Millennium Conference. IEEE International Conference on Robotics and Automation. Symposia Proceedings (Cat. No.00CH37065)*, vol. 2. San Francisco, CA, USA: IEEE, 2000, pp. 1734–1741. [Online]. Available: http://ieeexplore.ieee.org/document/844846/

[8] J. W. Romanishin, K. Gilpin, and D. Rus, "M-blocks: Momentum-driven, magnetic modular robots," in *2013 IEEE/RSJ International Conference on Intelligent Robots and Systems*. Tokyo: IEEE, Nov. 2013, pp. 4288–4295.

[9] B. Piranda and J. Bourgeois, "Designing a quasi-spherical module for a huge modular robot to create programmable matter," *Autonomous Robots*, vol. 42, no. 8, pp. 1619–1633, Dec. 2018. [Online].

[10] A. Sprowitz, S. Pouya, S. Bonardi, J. Van Den Kieboom, R. Mockel, A. Billard, P. Dillenbourg, and A. Jan Ijspeert, "Roombots: Reconfigurable Robots for Adaptive Furniture," *IEEE Computational Intelligence Magazine*, vol. 5, no. 3, pp. 20–32, Aug. 2010.

[11] S. A. Morin, Y. Shevchenko, J. Lessing, S. W. Kwok, R. F. Shepherd, A. A. Stokes, and G. M. Whitesides, "Using "Click-e-Bricks" to Make 3D Elastomeric Structures," *Advanced Materials*, vol. 26, no. 34, pp. 5991–5999, Sep. 2014.

[12] J.-Y. Lee, W.-B. Kim, W.-Y. Choi, and K.-J. Cho, "Soft Robotic Blocks: Introducing SoBL, a Fast-Build Modularized Design Block,"

15

IEEE Robotics & Automation Magazine, vol. 23, no. 3, pp. 30–41, Sep. 2016.

[13] D. Zappetti, S. Mintchev, J. Shintake, and D. Floreano, "Bio-inspired Tensegrity Soft Modular Robots," in *Biomimetic and Biohybrid Systems*, M. Mangan, M. Cutkosky, A. Mura, P. F. Verschure, T. Prescott, and N. Lepora, Eds. Cham: Springer International Publishing, 2017, vol. 10384, pp. 497–508.

[14] J. Ogawa, T. Mori, Y. Watanabe, M. Kawakami, M. N. I. Shiblee, and H. Furukawa, "MORI-A: Soft Vacuum-Actuated Module With 3D-Printable Deformation Structure," *IEEE Robotics and Automation Letters*, vol. 7, no. 2, pp. 2495–2502, Apr. 2022.

[15] R. H. Lee, E. A. B. Mulder, and J. B. Hopkins, "Mechanical neural networks: Architected materials that learn behaviors," *Science Robotics*, vol. 7, no. 71, p. eabq7278, Oct. 2022. [Online]. Available: https://www.science.org/doi/10.1126/scirobotics.abq7278

[16] B. Piranda and J. Bourgeois, "Datom: A deformable modular robot for building self-reconfigurable programmable matter," in *Distributed Autonomous Robotic Systems*, F. Matsuno, S.-i. Azuma, and M. Yamamoto, Eds. Cham: Springer International Publishing, 2022, pp. 70–81.

[17] T. Tucci, B. Piranda, and J. Bourgeois, "A distributed self-assembly planning algorithm for modular robots," in *Proceedings of the 17th International Conference on Autonomous Agents and MultiAgent Systems*, ser. AAMAS '18. Richland, SC: International Foundation for Autonomous Agents and Multiagent Systems, 2018, p. 550–558.